A.

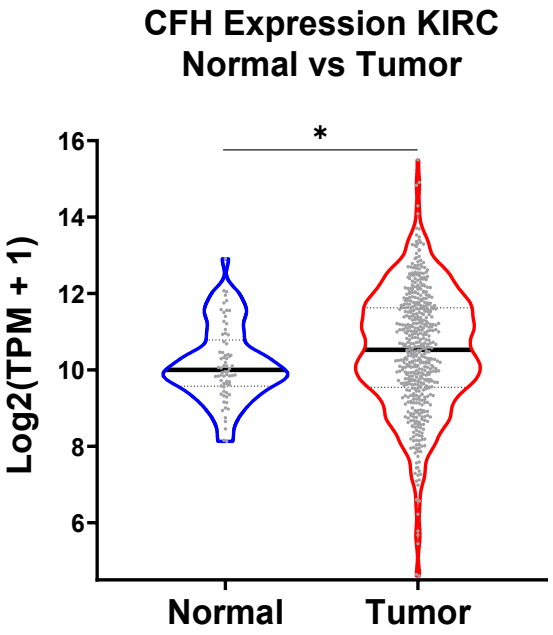

B.

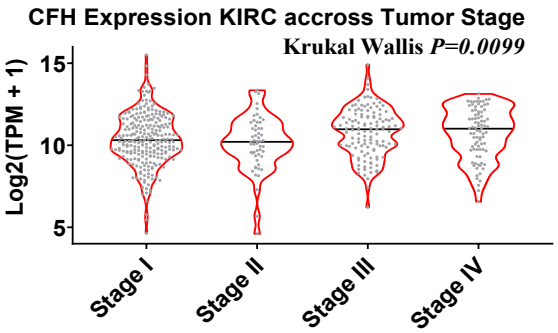

C.

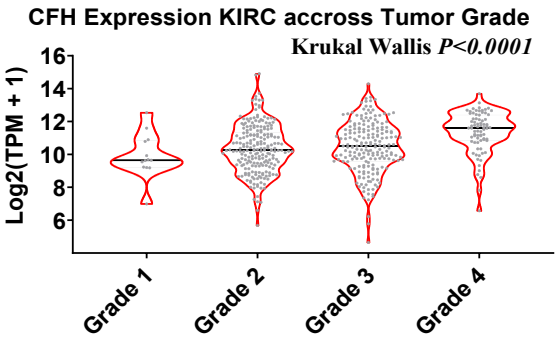

D.

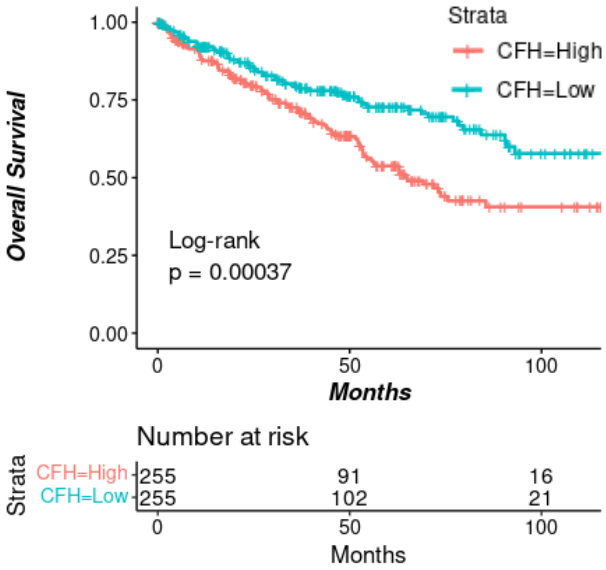

E.

Multivariate Cox model
CFH expression High vs Low KIRC

Overall Survival	HR(95% CI)	*P*
CFH (Z-score)	1.27 (1.07-1.51)	**0.00513**
Age (Years)	1.03 (1.02-1.05)	**2.66e-05**
Sex Male	1.01 (0.72-1.38)	0.976
Tumor Stage III/IV vs I/II	3.15 (2.24-4.45)	**5.52e-11**
Tumor Grade 3/4 vs 1/2	1.76 (1.21-2.54)	**0.003**

F.

Multivariate Cox model
CFH expression High vs Low KIRC

Progression-Free Survival	HR(95% CI)	*P*
CFH (Z-score)	1.24 (1.05-1.48)	**0.0116**
Age (Years)	1.00 (0.99-1.02)	0.39
Sex Male	1.46 (1.02-2.09)	**0.04**
Tumor Stage III/IV vs I/II	5.60 (3.82-8.19)	**< 2e-16**
Tumor Grade 3/4 vs 1/2	1.98 (1.34-2.91)	**5.8e-04**

G.

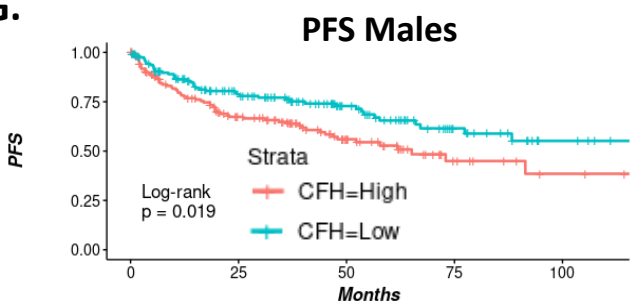

H.

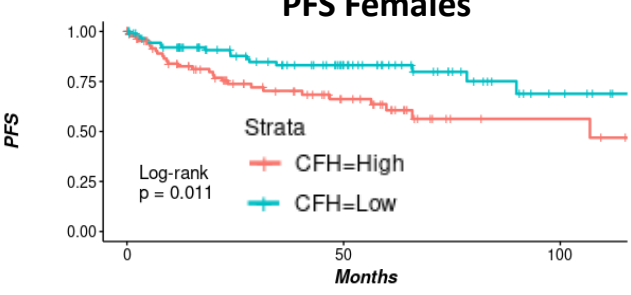

Supplementary Figure 1

Supplementary Figure 1: *CFH* expression is associated with ccRCC cancer progression. A. *CFH* expression in ccRCC tumors (n = 510) vs healthy adjacent tissue (n =70) from the KIRC TCGA cohort. *CFH* expression from the KIRC TCGA cohort (n = 510) across primary tumors with different **B.** tumor stages and **C.** tumor grades. **D.** Overall Survival Kaplan–Meier curves according to *CFH* expression in the KIRC TCGA cohort (n = 510). **E.** Multivariate cox regression analysis of clinical features and *CFH* expression for Overall Survival in the KIRC TCGA cohort. **F.** Multivariate Cox regression analysis of clinical features and *CFH* expression for Progression-Free Survival in the KIRC TCGA cohort. **G.** Progression-Free Survival Kaplan–Meier curves according to *CFH* expression (median cut-off) in the male patients of the KIRC TCGA cohort (n = 324). **H.** Progression-Free Survival Kaplan–Meier curves according to *CFH* expression (median cut-off) in the female patients of the KIRC TCGA cohort (n = 184). For the comparison of *CFH* expression levels between ccRCC vs healthy: *p-value ≤ 0,05, Mann–Whitney test.

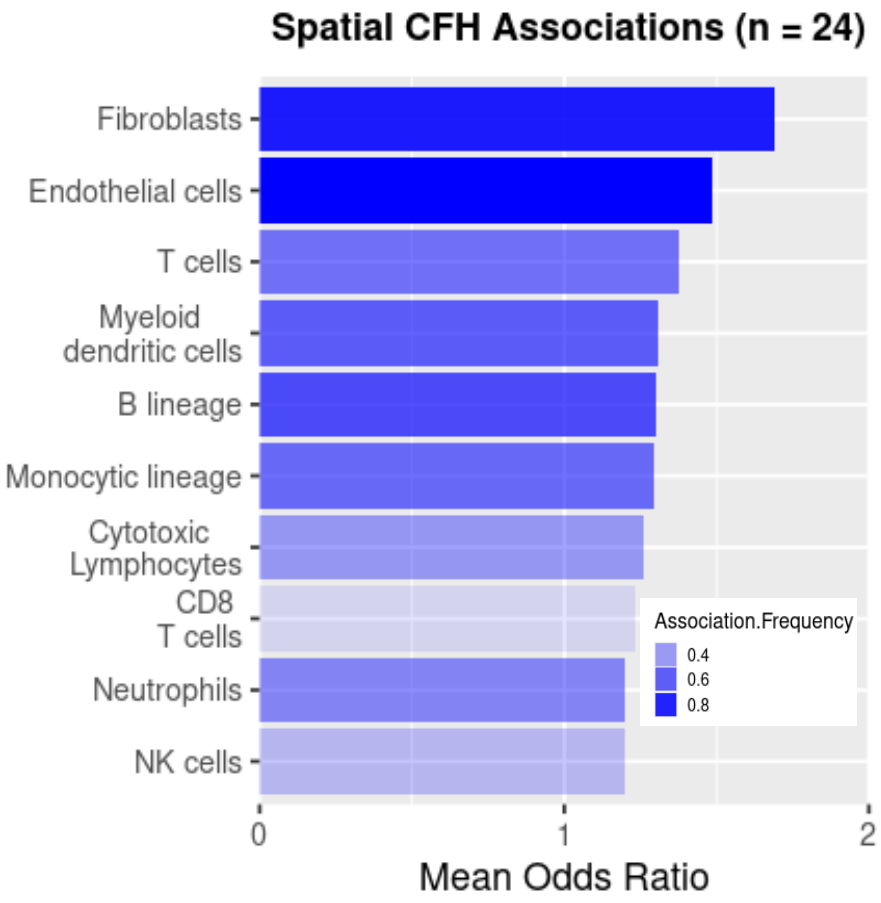

Supplementary Figure 2: Spatial *CFH* expression is associated with fibroblast signatures in ccRCC stroma. Barplot summarizing co-localization analysis across 24 ccRCC tumor sections (GSE175540) for the 10 different MCP Counter signatures tested. Co-localization was evaluated within each slide by a two-sided Fisher's exact test and the frequency of p-value ≤ 0,05 across slides is reported along with the estimated Odd's Ratio.

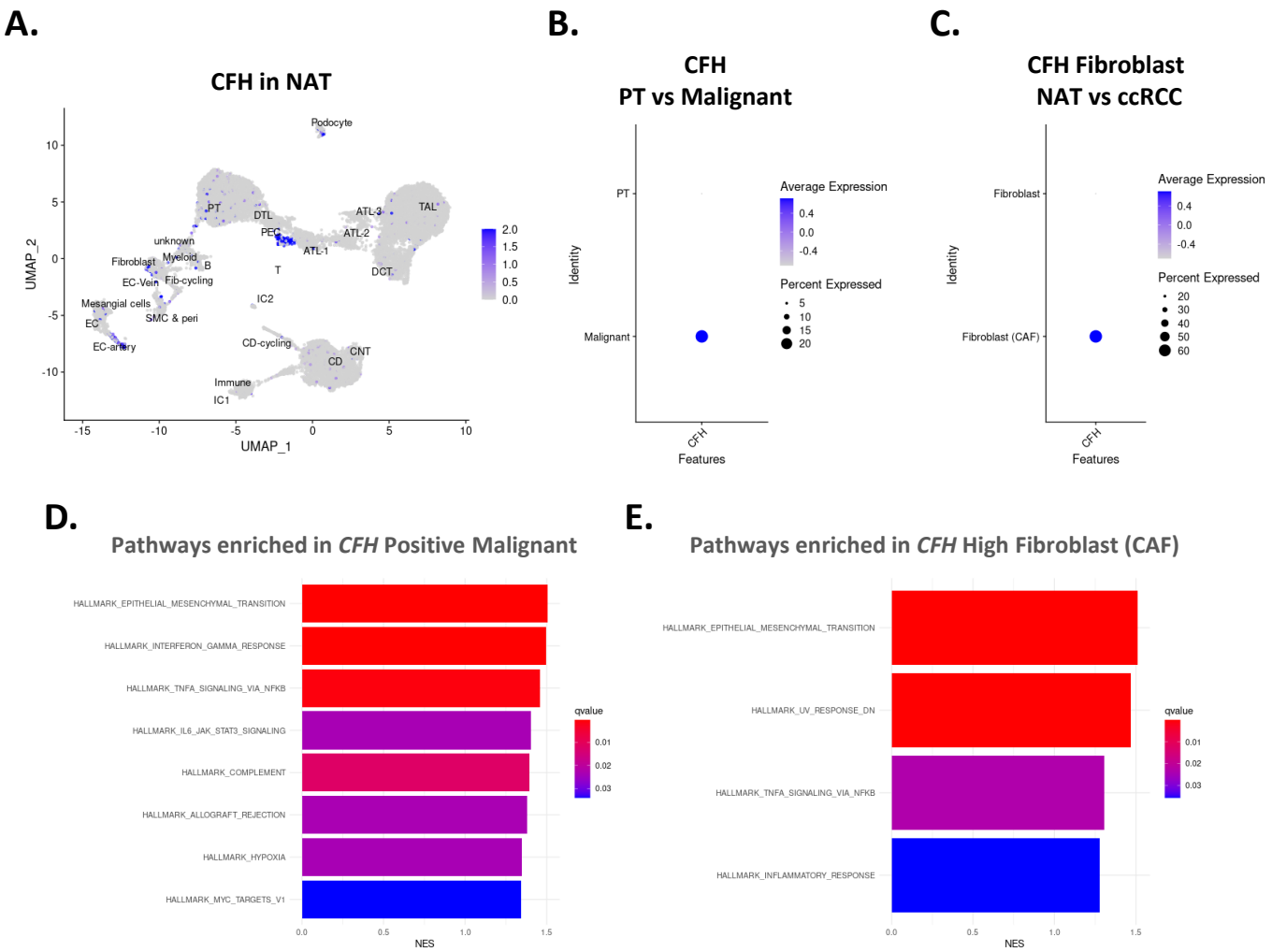

Supplementary Figure 3: *CFH* expression is induced in ccRCC cancer associated fibroblasts and malignant cells and associates with pro-inflammatory signaling. A. UMAP displaying normal adjacent tissue *CFH* expression across labelled Seurat clusters from two ccRCC patients. Dot plot displaying scaled mean expression levels (dot color) and percentage of cells (dot size) expressing *CFH* in **B.** proximal tubular cells vs. malignant cells, and in **C.** fibroblasts vs. cancer associated fibroblasts. Gene set enrichment analysis of hallmark pathways associated with *CFH* expression in **D.** malignant cells and **E.** cancer associated fibroblasts.

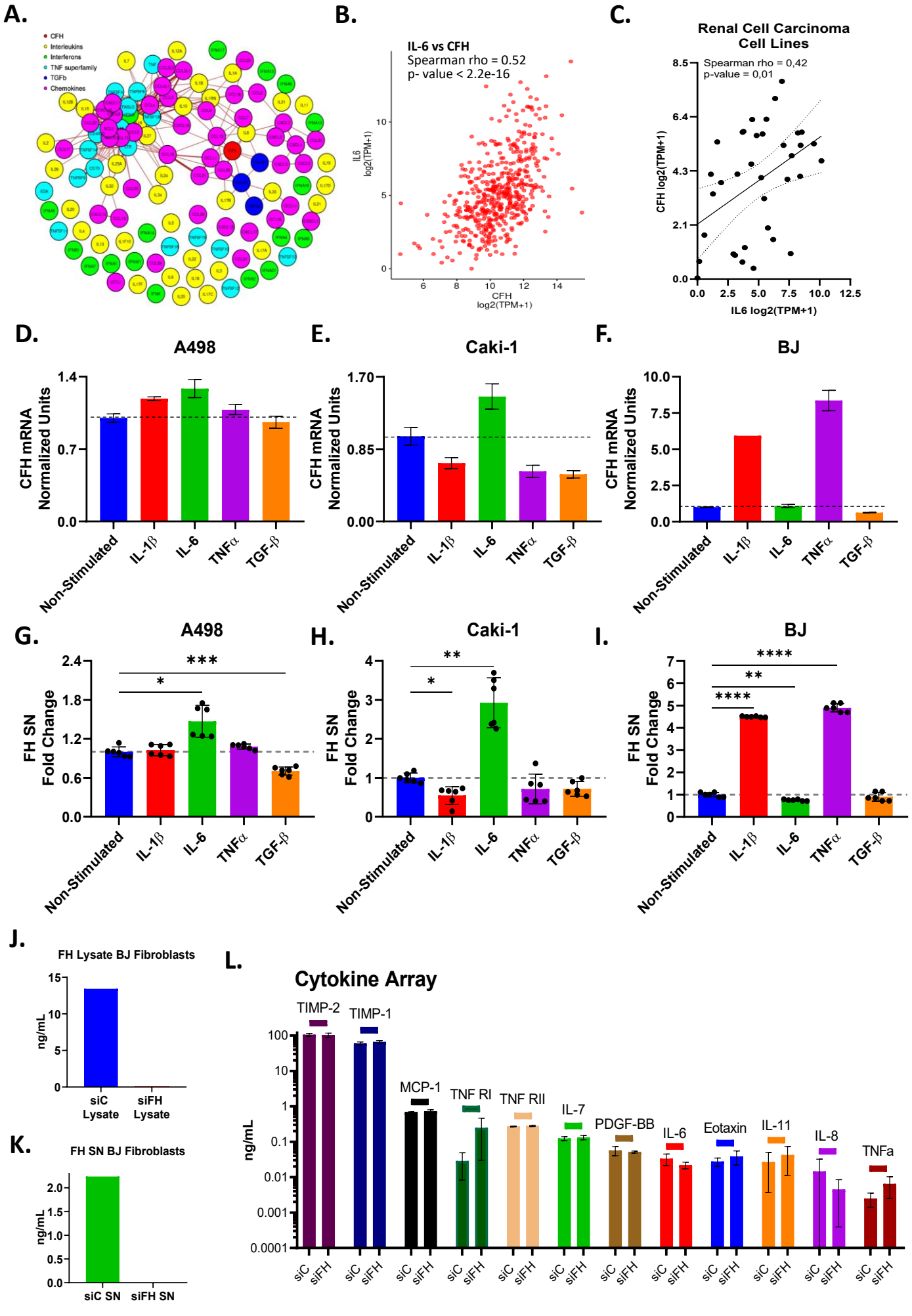

Supplementary Figure 4

Supplementary Figure 4: *CFH* expression is stimulated by pro-inflammatory cytokines in ccRCC. A. Correlation network depicting gene expression relationships (absolute spearman's rho > 0.45 and adjusted BH p-value < 0.05) between *CFH* and various cytokines (data from the KIRC TCGA cohort, n = 510). **B.** Positive gene expression correlation between *IL6* and *CFH* in primary ccRCC tumors from KIRC TCGA cohort. **C.** Positive gene expression correlation between *IL6* and *CFH* in RCC cell lines (data sourced from "DepMap Public 23Q4"). Quantigene *CFH* RNA levels in 24 hours cytokine stimulated **D.** A498 ccRCC cells, **E.** Caki-1 ccRCC cells and **F.** BJ fibroblasts. FH protein levels in supernatants (SN) of 24 hours cytokine stimulated **G.** A498 ccRCC cells, **H.** Caki-1 ccRCC cells and **I.** BJ fibroblasts. FH protein concentration in siC vs siFH BJ fibroblast's **J.** lysates and **K.** SN determined by ELISA. **L.** SN cytokine array analysis of siC vs siFH treated BJ fibroblast 96 hours post-transfection. For the comparison of FH protein levels in the SN of cytokine stimulated and non-stimulated cells: * p-value ≤ 0,05, ** p-value ≤ 0,01, *** p-value ≤ 0,001, **** p-value < 0,0001, Brown-Forsythe and Welch ANOVA tests plus *post-hoc* Tamhane's T2 multiple comparisons test.

A.

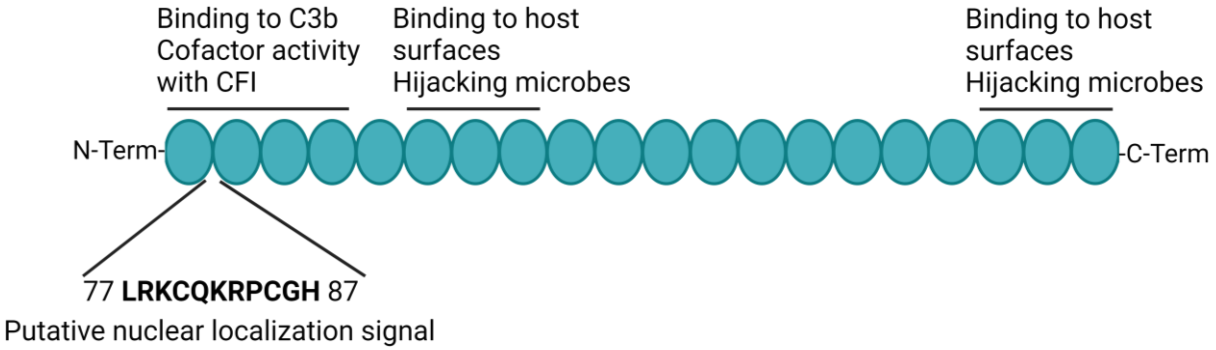

Predicted monopartite NLS		
Pos.	Sequence	Score
77	LRKCQKRPCGH	6.5

B.

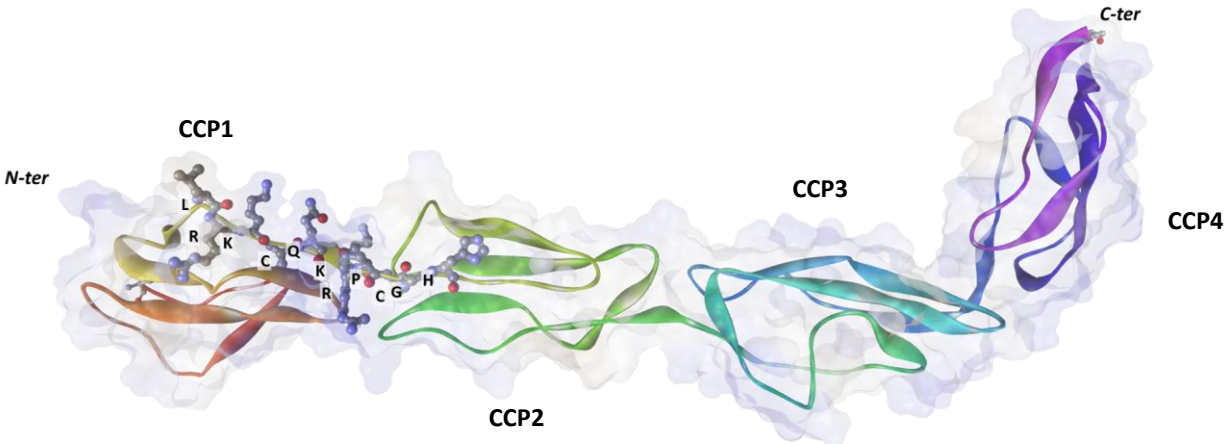

Supplementary Figure 5: FH sequence contains a putative nuclear localisation signal (NLS) in its N-terminal region. A. FH scheme highlighting the location of the NLS signal between the CCP1 and CCP2 domains of FH. The output from the bioinformatics software cNLS Mapper identifying a NLS sequence at the N-terminal region of FH (FH aminoacid sequence was obtained from Uniprot, accession number P08603-1) is presented. **B.** *In silico* evaluation of the FH NLS sequence. FH CCP1-CCP4 crystal structure from PDB (2WII) highlighting the FH NLS sequence. Visualization done by Discovery Studio visualizer. The structure of FH CCP1-CCP4 is shown using a solid ribbon schematic and colored in a rainbow and the NLS sequence is represented with atom-colored balls and sticks, labeled with the identifiers of the constituent amino acids.

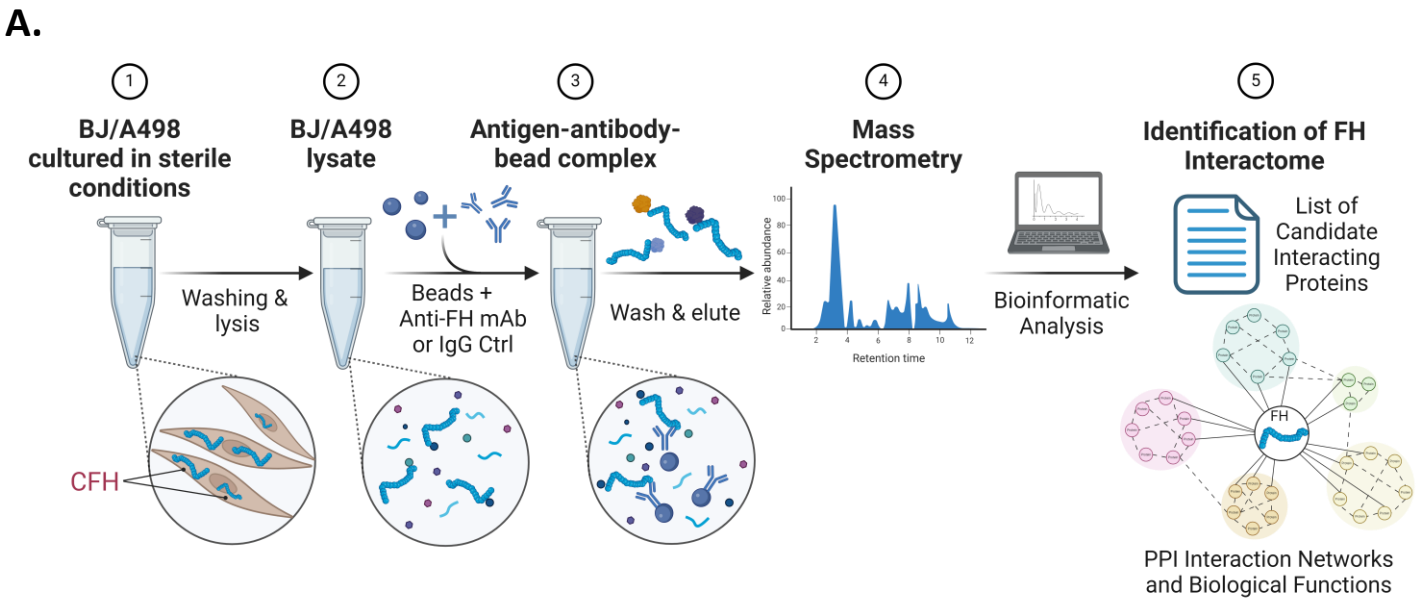

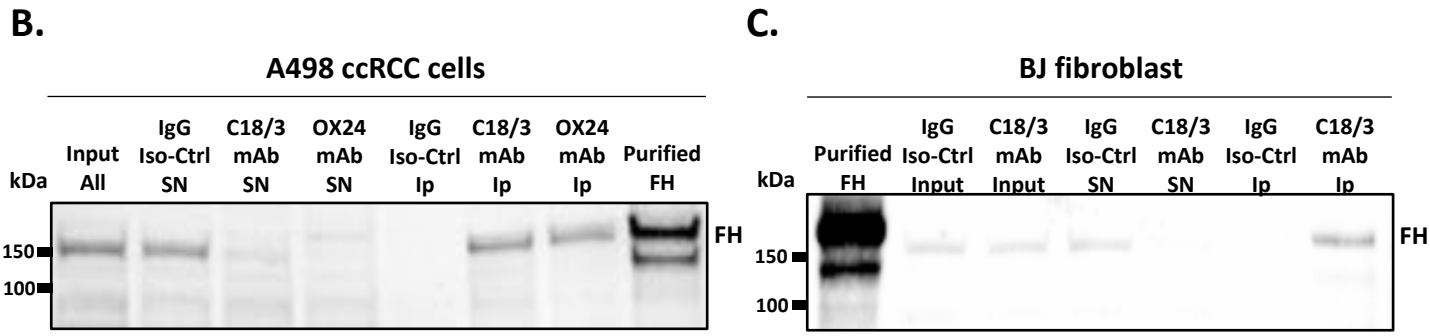

Supplementary Figure 6: Intracellular FH co-immunoprecipitation strategy with various anti-FH mAbs. A. Experimental workflow: either A498 lysates or BJ lysates were incubated with anti-C-terminus FH mAb C18/3, anti-N-terminus FH mAb OX24 (only for A498) or unspecific isotype control immunoglobuling G (Neg Ctrl). Immunoprecipitation was then performed on protein A/G beads and proteins were eluted and processed before data acquisition by mass-spectrometry followed by bioinformatics analysis of the interacting candidates. **B.** FH western blot validating intracellular FH immunoprecipitation with the mAb C18/3 and the mAb OX24 in A498 lysates. **C.** FH western blot validating intracellular FH immunoprecipitation with the mAb C18/3 in BJ lysates. Input: starting lysate material; SN: supernatant; IP: immunoprecipitates.

A.

A498
Intracellular FH-interacting candidates
(Anti-C-terminal FH C18/3 mAb)

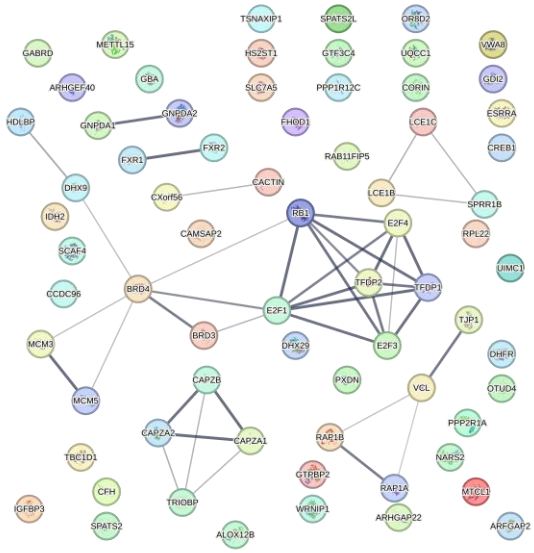

B.

BJ
Intracellular FH-interacting candidates
(Anti-C-terminal FH C18/3 mAb)

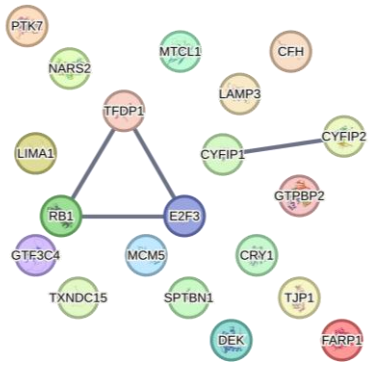

C.

A498
Intracellular FH-interacting candidates
(Anti-N-terminal FH OX24 mAb)

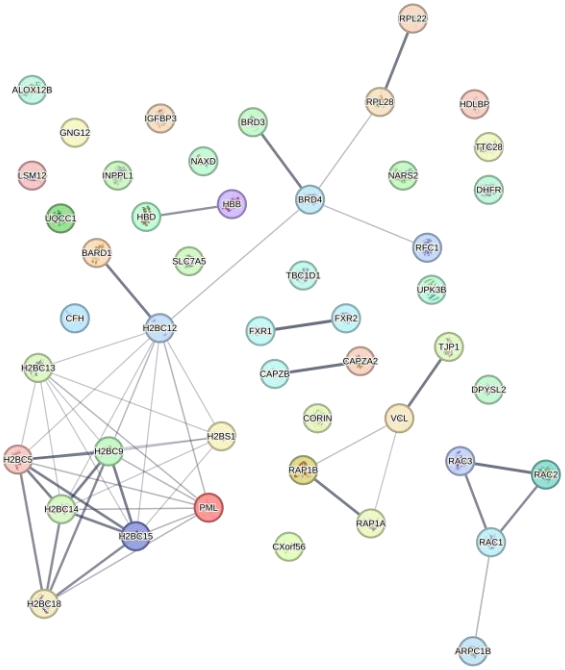

D.

A498 FH Interactor Enrichment Analysis
(OX24 mAb enriched candidates)

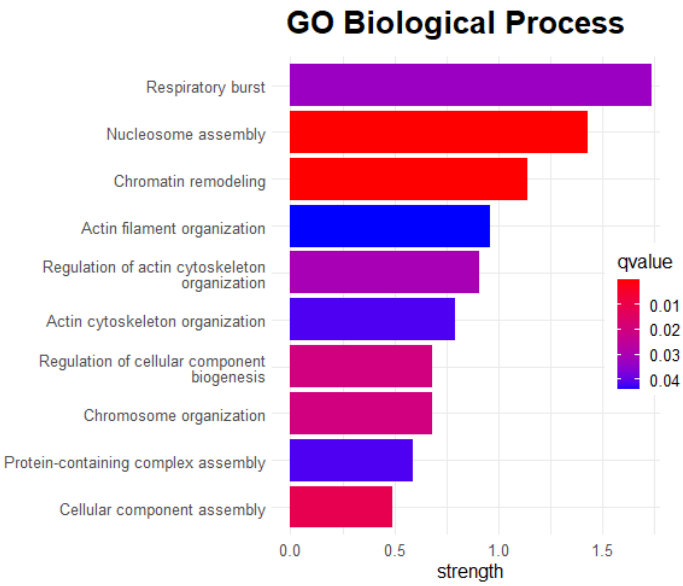

Supplementary Figure 7: N-terminal FH interacts with transcription factors associated to the RB1/E2F pathway whereas C-terminal FH interacts with histones. Protein-protein interaction network analysis of FH interacting proteins generated by immunoprecipitation with anti-C-terminal FH mAb C18/3 for **A.** A498 ccRCC cells and **B.** BJ fibroblasts; STRING Tool, physical subnetwork with at least 0.4 confidence. **C.** Protein-protein interaction network analysis of FH interacting proteins generated by immunoprecipitation with anti-N-terminal FH mAb OX24 in A498 cells; STRING Tool, physical subnetwork with at least 0.4 confidence. **D.** Top 10 gene-ontology pathways (biological processes) for FH interacting proteins generated by immunoprecipitation with anti-N-terminal FH mAb OX24 in A498 ccRCC cells.

A.

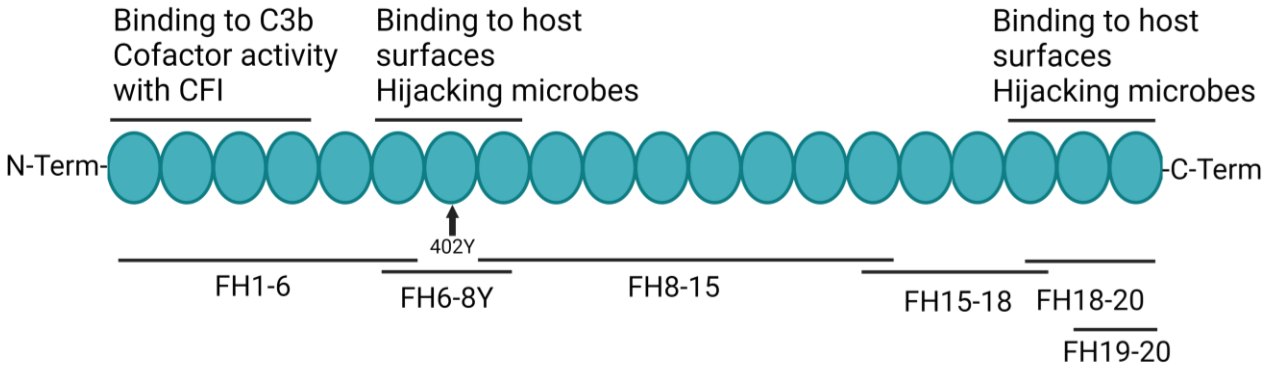

B.

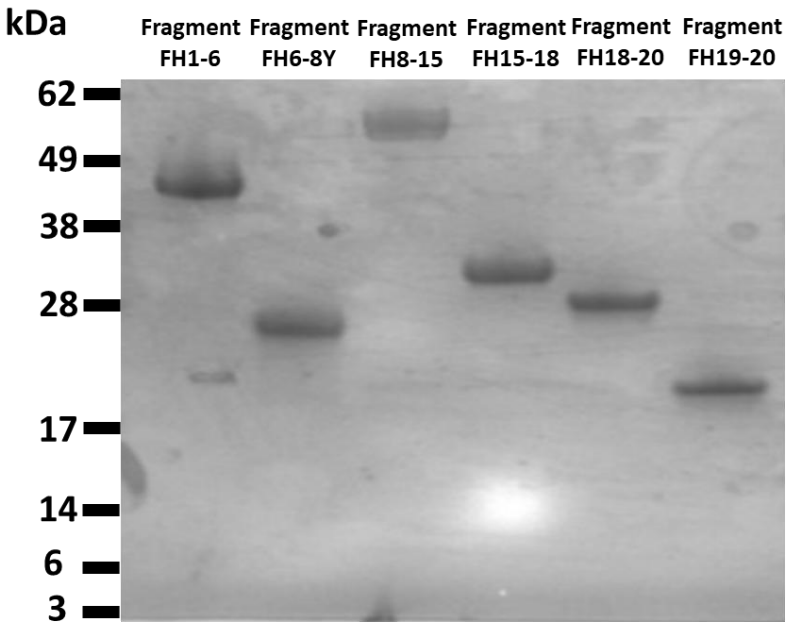

Supplementary Figure 8: Recombinant FH fragments. A. Scheme representing the location of the recombinant FH fragments within FH. **B**. SDS-PAGE analysis of the recombinant fragments of FH used for SPR experiments.

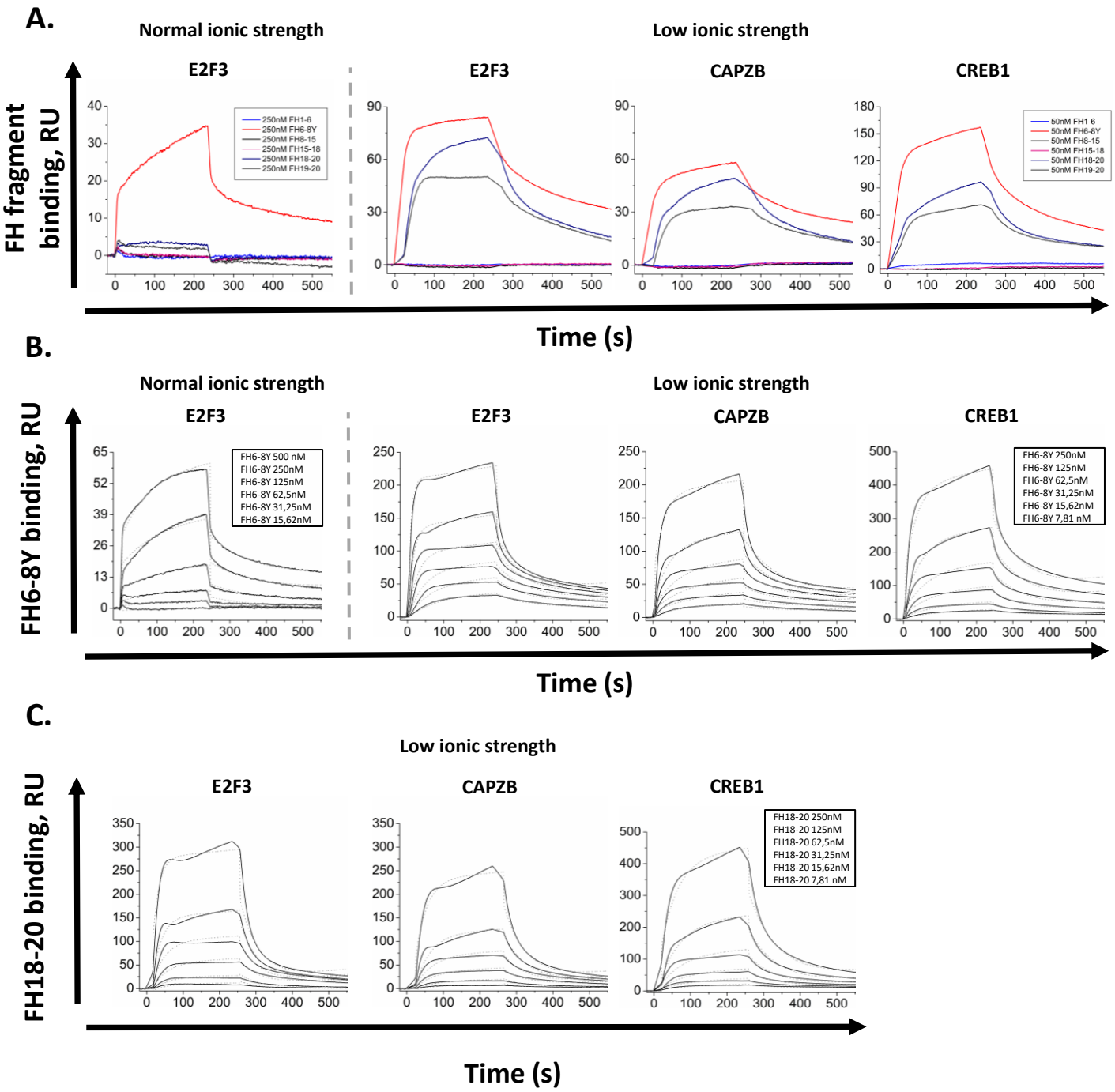

Supplementary Figure 9: Characterization of the interacting FH regions and kinetics. A. SPR analysis using different FH fragments at 250nM concentration and normal ionic strength (left, dashed lined), or 50nM concentration and low ionic strength (right, dashed line). **B.** Kinetic SPR analysis using recombinant FH6-8Y at concentrations ranging from 15.62nM to 500nM, two-fold dilutions and normal ionic strength (left, dashed lined), and FH6-8Y at concentrations ranging from 7.81nM to 250nM, two-fold dilutions and low ionic strength (right, dashed line). **C.** Kinetic SPR analysis using recombinant FH18-20 at concentrations ranging from 7.8nM to 250nM, two-fold dilutions. FH fragments were injected on the respective FH interacting candidate coated chip for 240 s followed by 240 s dissociation. A 1:1 interaction with a drifting baseline curve was fitted to calculate kinetic parameters. **B,C.** The straight line represents the measured signal. The dotted one represents the kinetic fit. Curves from high to low RU values match the FH concentrations used (high FH, high RU values).

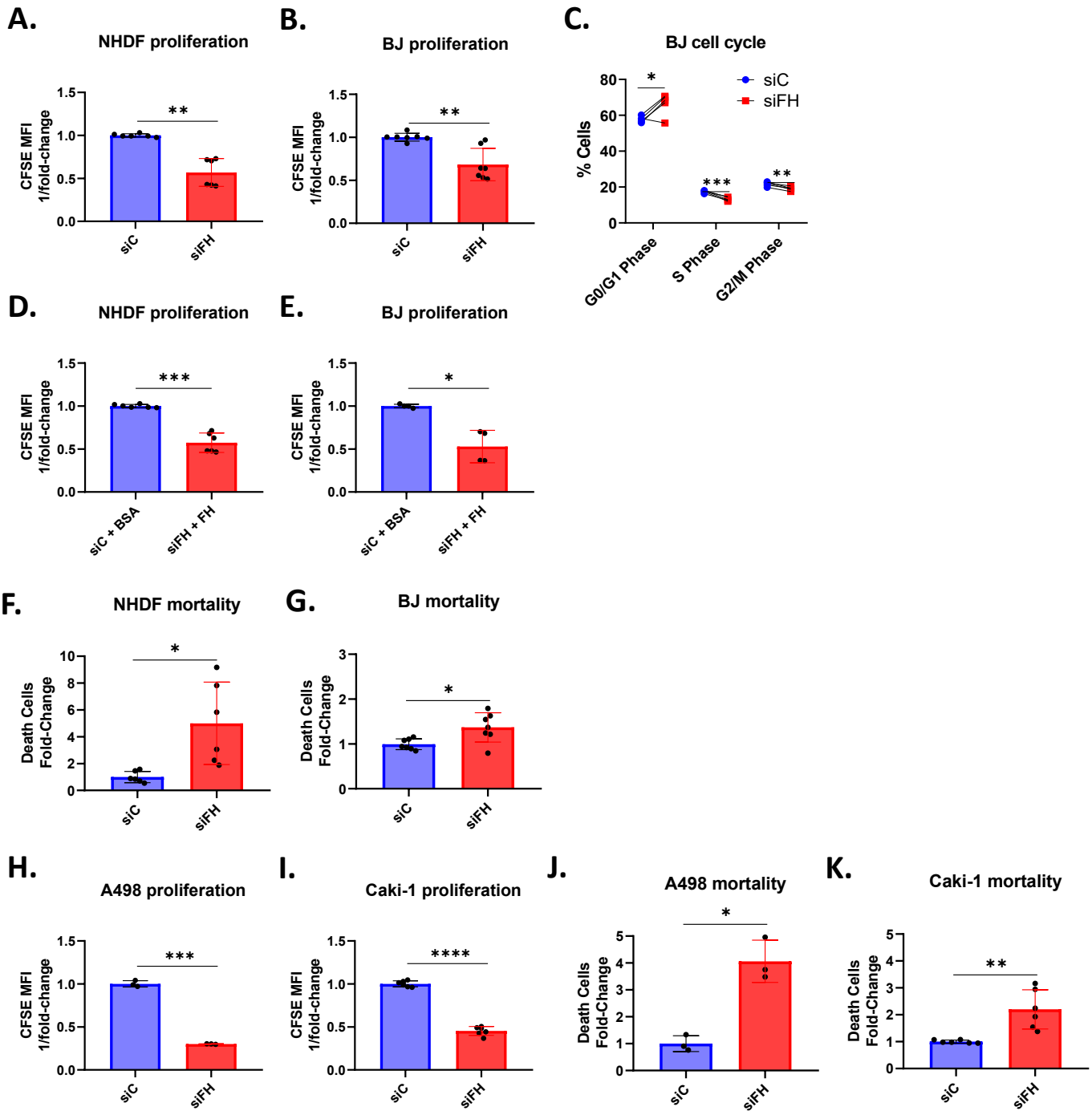

Supplementary Figure 10: *CFH* silencing reduces cell proliferation, cell cycle progression and viability. Evaluation of proliferation (CFSE assay) in siC vs siFH treated **A.** NHDF fibroblasts and **B.** BJ fibroblasts. **C.** Percentage of BJ fibroblasts in each phase of the cell-cycle (G0/G1, S, G2/M) determined by flow cytometry analysis of PI staining. Evaluation of proliferation (CFSE assay) in siC vs siFH treated **D.** NHDF fibroblasts and **E.** BJ fibroblasts with 10 µg/mL of purified FH (siFH) or BSA (siC). Evaluation of viability (DAPI death cell staining) by flow cytometry in siC vs siFH treated **F.** NHDF fibroblasts and **G.** BJ fibroblasts. Evaluation of proliferation (CFSE assay) in siC vs siFH treated **H.** A498 ccRCC cells and **I.** Caki-1 ccRCC cells. Evaluation of viability (DAPI death cell staining) by flow cytometry in siC vs siFH treated **J.** A498 ccRCC cells and **K.** Caki-1 ccRCC cells. For cell proliferation, data is shown as inversed Fold Change of CFSE geometric means and for mortality data is represented as the Fold Change of DAPI stained dead cells. For all the comparisons between siC vs siFH: * p-value ≤ 0,05, ** p-value ≤ 0,01, *** p-value ≤ 0,001, Welch's t-test.

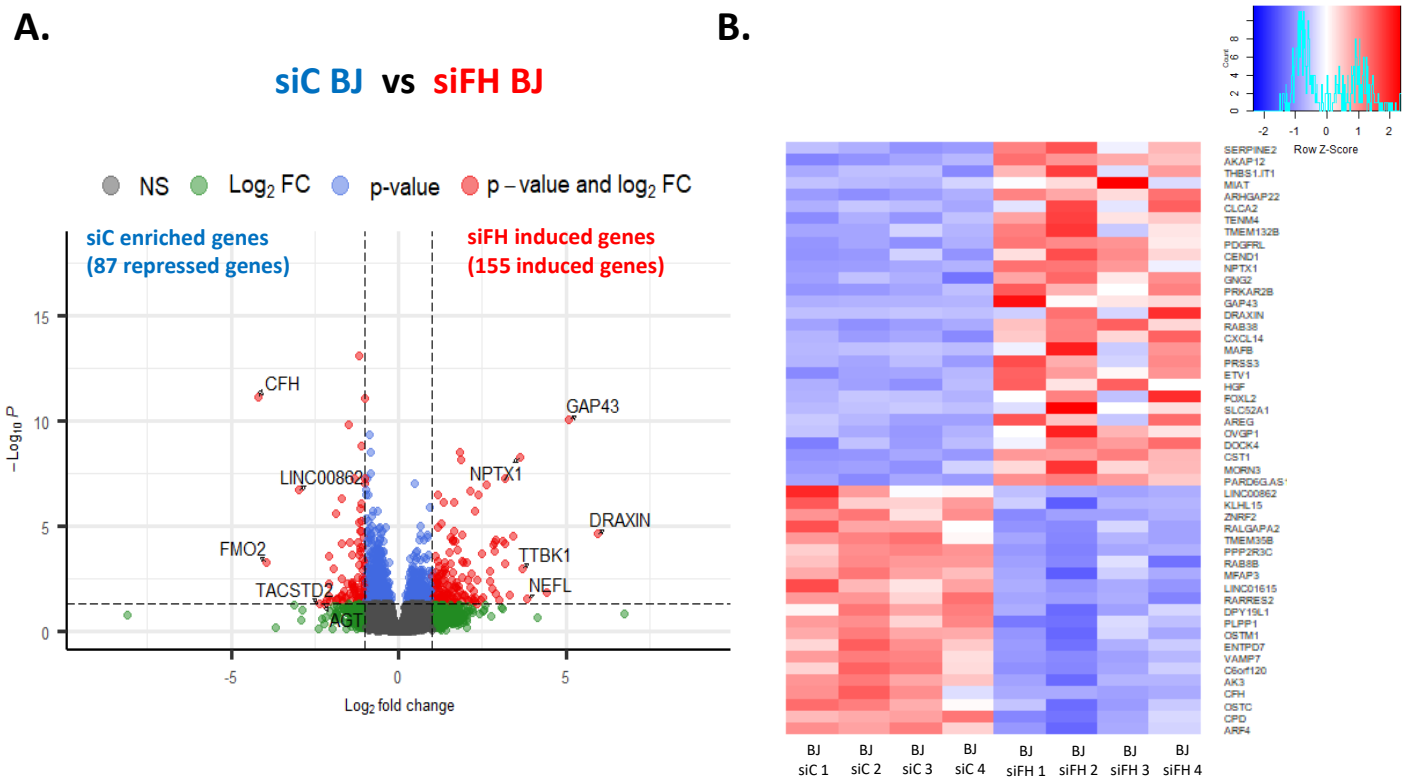

Supplementary Figure 11: FH silencing modifies the BJ fibroblast's transcriptome. A. Volcano plot depicting the results of differential expression analysis between BJ siFH (n = 4) and BJ siC cells (n = 4); red points represent genes with an absolute log2 fold change > 1 and adjusted p-value < 0.05. **B.** Heatmap for the top 50 differentially expressed genes after FH silencing in BJ fibroblasts; rows are genes and columns experimental replicates. Data are scaled and centered per gene and the range was truncated ±2.5.

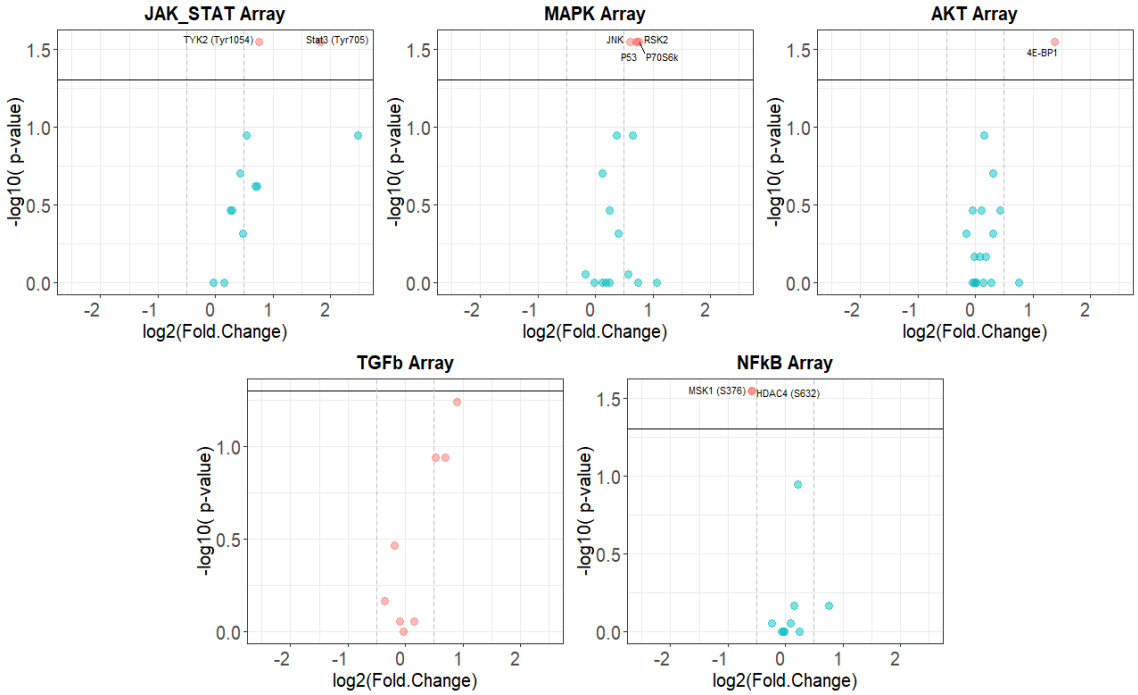

Supplementary Figure 12: *CFH* silencing in BJ fibroblasts does not alter the JAK-STAT, MAPK, AKT, TGF-β and NF-kβ pathways. Volcano plots representing changes in protein phosphorylation (siC vs siFH) for silenced BJ fibroblasts. Annotated proteins correspond to phosphorylation changes of at least 0.5 Fold Change and p-value < 0.05 (one sample t-test).

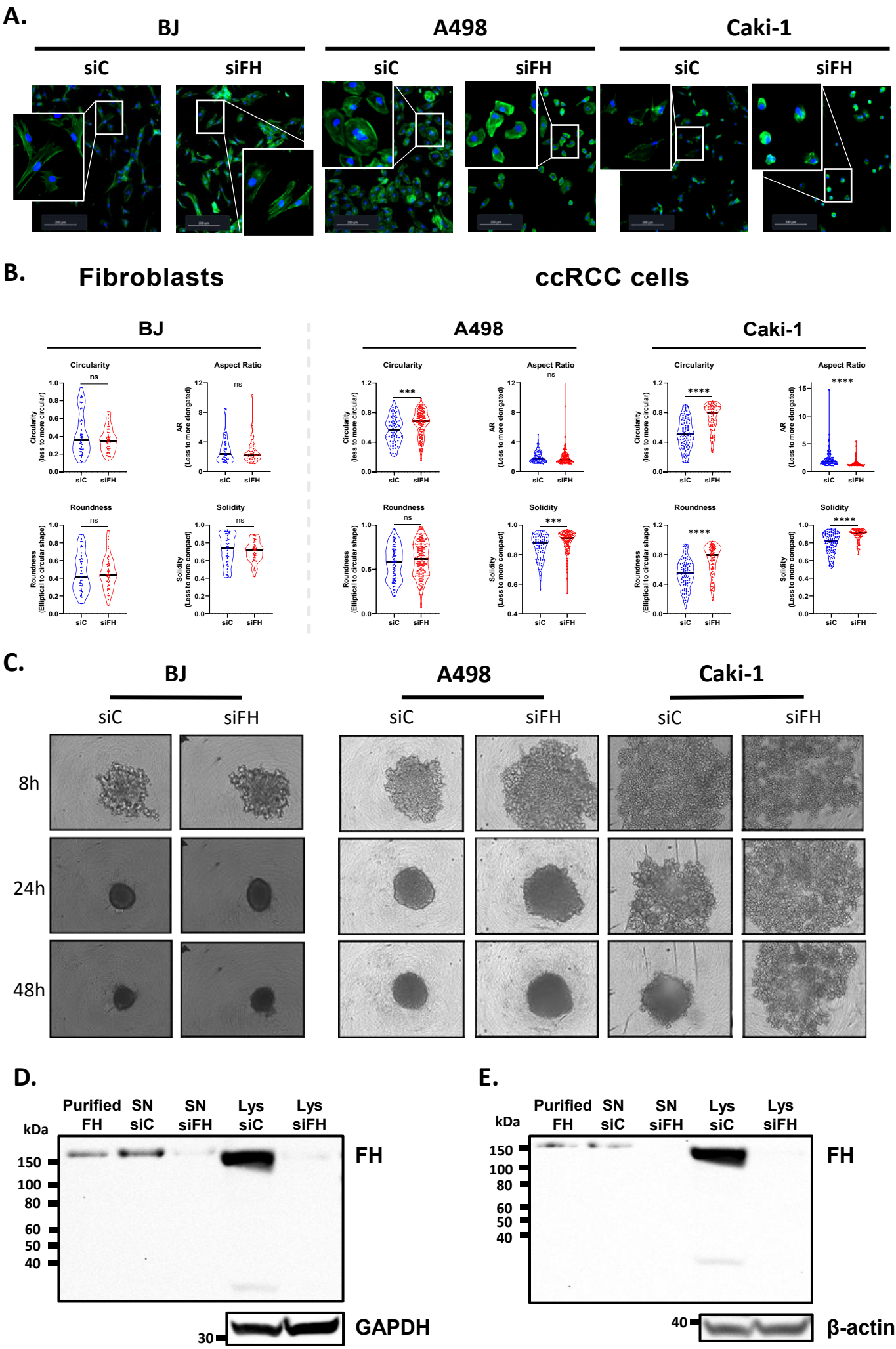
A.
BJ
A498
Caki-1
siC
siFH
siC
siFH
siC
siFH
B.
Fibroblasts
ccRCC cells
BJ
A498
Caki-1
Circularity
Aspect Ratio
Roundness
Solidity
ns
***
****
siC
siFH
C.
BJ
A498
Caki-1
siC
siFH
8h
24h
48h
D.
Purified FH
SN siC
SN siFH
Lys siC
Lys siFH
kDa
150
100
80
60
50
40
FH
30
GAPDH
E.
Purified FH
SN siC
SN siFH
Lys siC
Lys siFH
kDa
150
100
80
60
50
40
FH
40
β-actin

Supplementary Figure 13: FH silencing impairs F-actin cytoskeleton and spheroid forming capacity of ccRCC cells independently from β-actin expression. Immunofluorescence phalloidin staining (green) of **A.** siC or siFH treated A498 ccRCC cells (left), Caki-1 ccRCC cells (center) and BJ fibroblasts (right), **B.** Analysis of morphological parameters comparing siC vs siFH BJ fibroblasts (left), A498 ccRCC cells (center) and Caki-1 ccRCC cells (right). **C.** Evaluation of spheroid forming capacity of siC vs siFH treated BJ fibroblasts (left), A498 ccRCC cells (center) and Caki-1 ccRCC cells (right) across three different time points, 8, 24 and 48 hours since the beginning of the assay. FH western blot with plasma purified FH along with lysates and SN from A498 ccRCC cells employing **D.** GAPDH as a control, or **E.** β-actin as a control.

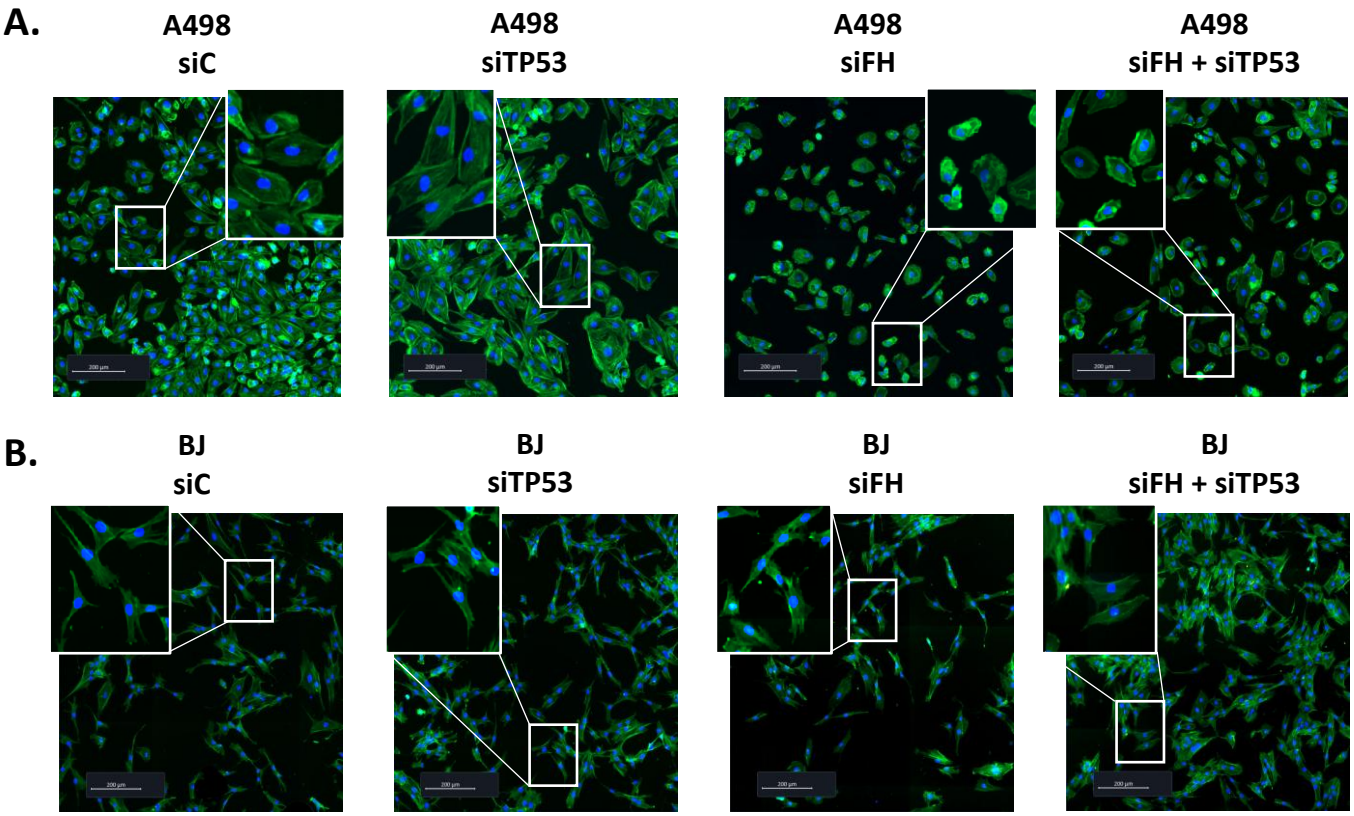

Supplementary Figure 14: FH silencing impairs F-actin cytoskeleton of ccRCC cells in a p53-independent manner. Immunofluorescence phalloidin staining (green) of **A.** siC (left), siTP53 (left center), siFH (right center) and siTP53 + siFH (right) treated A498 cells, and **B.** siC (left), siTP53 (left center), siFH (right center) and siTP53 + siFH (right) treated BJ fibroblasts.

A.

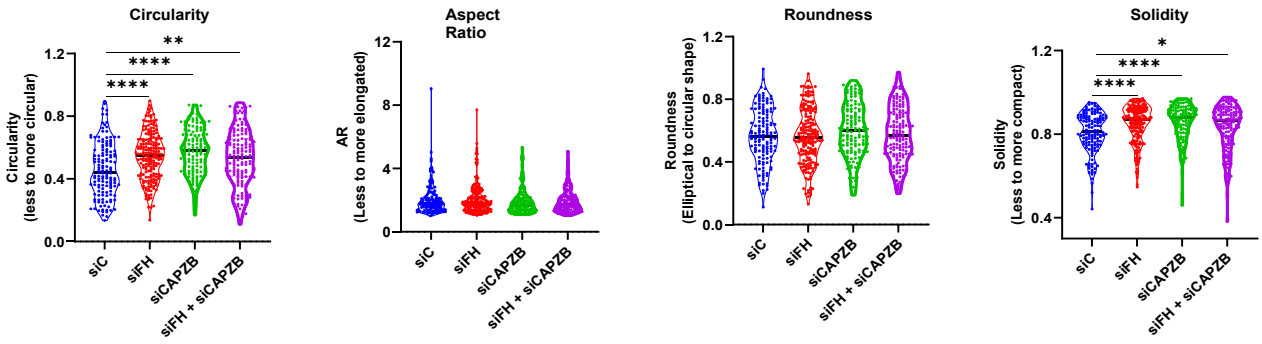

B.

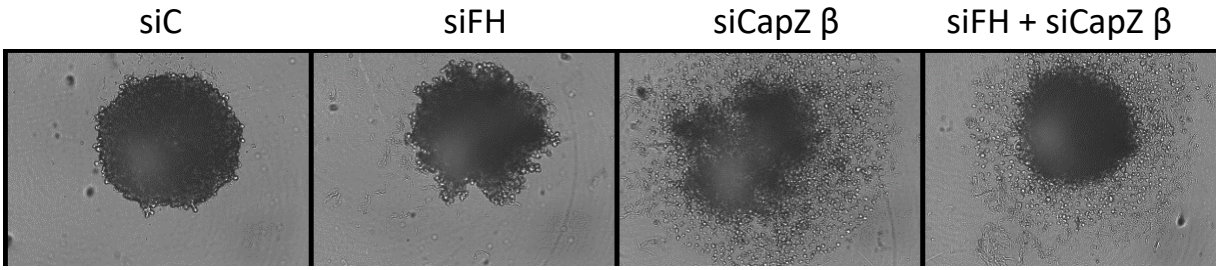

Supplementary Figure 15: si*FH* and si*CAPZB* alterations of F-actin cytoskeleton and spheroid formation are not additive in ccRCC cells. A. Analysis of morphological parameters comparing siC vs siFH vs siCAPZB vs siFH + siCAPBZ treated cells. **B.** Evaluation of spheroid forming capacity of siC vs siFH vs siCAPZB vs siFH + siCAPBZ treated cells at 12 hours since the beginning of the assay (4 replicates per condition shown).

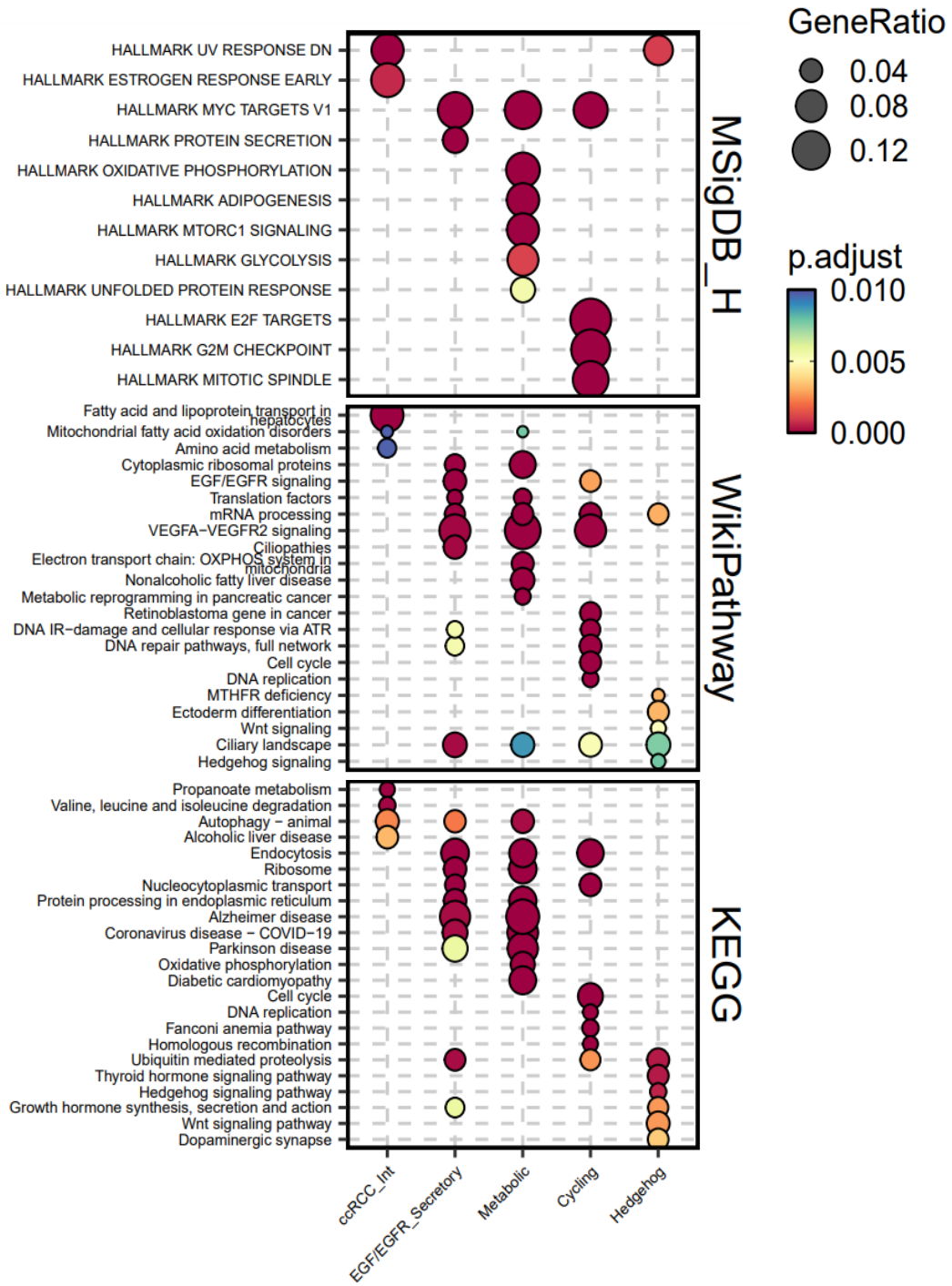

Supplementary Figure 16: Over representation analysis (ORA) of differentially overexpressed genes reveals the biological characteristics of the different malignant cell states. ORA analysis results (Hallmark genesets, top; WikiPathway, middle; KEGG, bottom) of pathways overrepresented in the different malignant cell subclusters. Color represents adjusted p-value and dot size gene ratio for the specified pathway.

Supplementary Figure 17: Over representation analysis (ORA) identifies common and branch-specific modulated pathways across pseudotime**.** ORA analysis (Hallmark genesets) of differentially expressed genes across pseudotime in the two trajectory branches in the malignant cell cluster. Dot plot showcasing adjusted p-values as colors and gene ratios as dot size.

A.

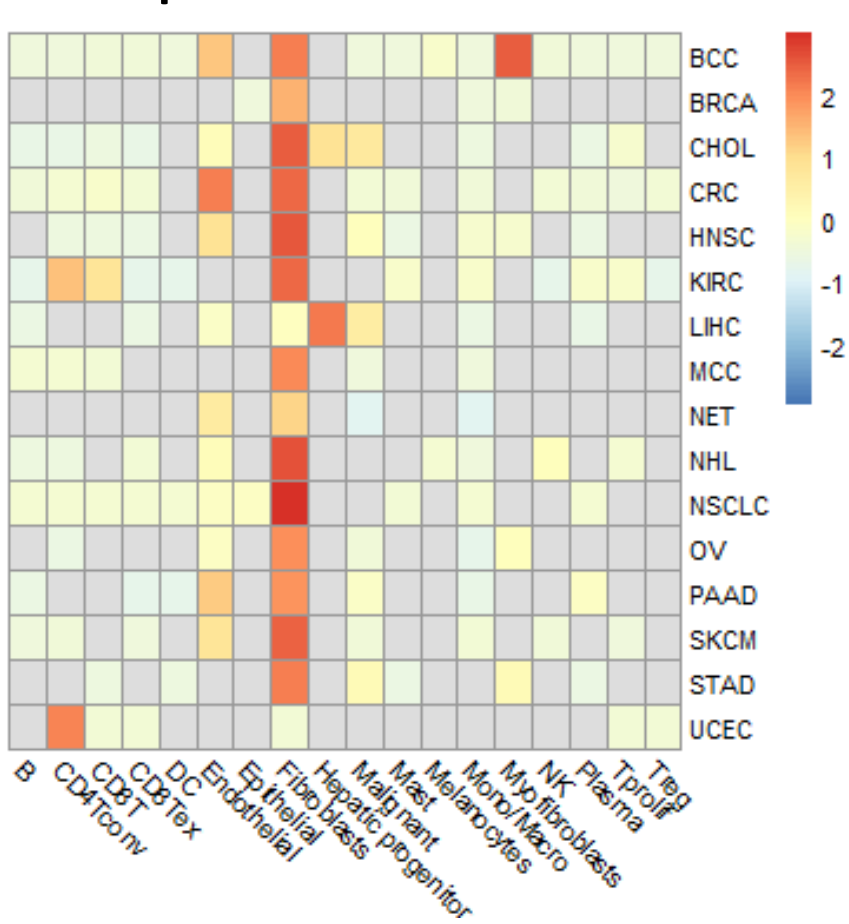

B.

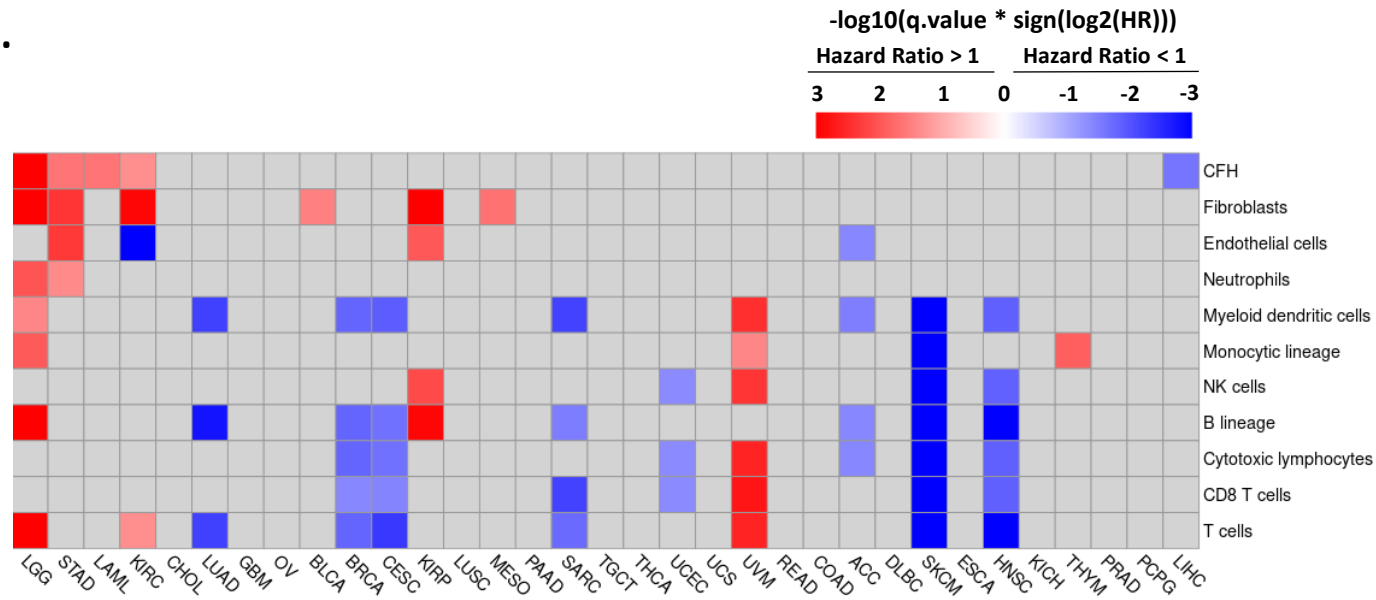

Supplementary Figure 18: *CFH* expression prognosis associates with fibroblast signatures across cancers.

Supplementary Figure 18: *CFH* expression prognosis associates with fibroblast signatures across cancers. A. Heatmap representing *CFH* expression across cell types in 16 different types of cancer (scRNAseq data from Tumor Immune Single-Cell Hub, TISCH). **B.** Overall Survival meta-analysis for the univariate Cox proportional hazards model prognostic value of *CFH* expression and MCP-counter scores across the different TCGA cancer cohorts. Red represents hazard ratios bigger than 1 (unfavorable prognostic impact), blue hazard ratios lower than 1 (favorable prognostic impact) and grey represents non-significant hazard ratios after adjustment for FDR. BCC: basal cell carcinoma; CRC: colorectal cancer; MCC: merkel cell carcinoma; NET: neuroendocrine tumor; NHL: Non-Hodgkin lymphoma; NSCLC: non-small cell lung cancer; LGG: Brain Lower Grade Glioma; STAD: Stomach adenocarcinoma; LAML: Acute Myeloid Leukemia; KIRC: Kidney renal clear cell carcinoma; CHOL: Cholangiocarcinoma; LUAD: Lung adenocarcinoma; GBM: Glioblastoma multiforme; OV: Ovarian serous cystadenocarcinoma; BLCA: Bladder Urothelial Carcinoma; BRCA: Breast invasive carcinoma; CESC: Cervical squamous cell carcinoma and endocervical adenocarcinoma; KIRP: Kidney renal papillary cell carcinoma; LUSC: Lung squamous cell carcinoma; MESO: Mesothelioma; PAAD: Pancreatic adenocarcinoma; SARC: Sarcoma; TGCT: Testicular Germ Cell Tumors; THCA: Thyroid carcinoma; UCEC: Uterine Corpus Endometrial Carcinoma; UCS: Uterine Carcinosarcoma; UVM: Uveal Melanoma; READ: Rectum adenocarcinoma; COAD: Colon adenocarcinoma; ACC: Adrenocortical carcinoma; DLBC: Lymphoid Neoplasm Diffuse Large B-cell Lymphoma; SKCM: Skin Cutaneous Melanoma; ESCA: Esophageal carcinoma; HNSC: Head and Neck squamous cell carcinoma; KICH: Kidney Chromophobe; THYM: Thymoma; PRAD: Prostate adenocarcinoma; PCPG: Pheochromocytoma and Paraganglioma; LIHC: Liver hepatocellular carcinoma.